Supplement of Geosci. Model Dev., 18, 4915–4933, 2025
https://doi.org/10.5194/gmd-18-4915-2025-supplement

Geoscientific Model Development
Open Access
EGU

Supplement of

Spatially varying parameters improve carbon cycle modeling in the Amazon rainforest with ORCHIDEE r8849

Lei Zhu et al.

Correspondence to: Philippe Ciais (philippe.ciais@lsce.ipsl.fr), Yitong Yao (yyao2@caltech.edu), and Wei Li (wli2019@tsinghua.edu.cn)

This file includes:

Supplementary Texts S1-S3

Supplementary Figures S1-S24

Supplementary Tables S1-S4

References

Supplementary Texts

Text S1: Modifications made based on ORCHIDEE r8240

Text S1.1 NPP allocation

This ORCHIDEE version (r8240) is not well calibrated in the tropical region. Previous study mainly focuses on the calibration of NEE or GPP, but ignore the carbon allocation (Bastrikov et al., 2018; Raoult et al., 2024). The NPP allocation scheme in the ORCHIDEE model follows the pipe model theory (Shinozaki et al., 1964; Naudts et al., 2015), which assumes that the production of one unit of leaf mass requires a proportional amount of sapwood for water transport from roots to leaves, along with a corresponding proportion of roots for water uptake from the soil. The pipe model follows the following formulas (Naudts et al., 2015):

$$M_l = \frac{f_{KF} \times M_s}{d_h} \quad (s1)$$

$$M_r = \frac{M_s}{k_{sar} \times d_h} \quad (s2)$$

where M_l, M_s and M_r are leaf, sapwood, and root carbon mass, d_h is the tree height, f_{KF} is the scaling factor to convert sapwood mass into leaf mass, k_{sar} is the scaling factor to convert sapwood mass into root mass. f_{KF} and k_{sar} are calculated as:

$$f_{KF} = \frac{k_{lsmin} + f_{Pgap} \times (k_{lsmax} - k_{lsmin})}{k_{sla} \times k_{\rho s} \times f_{tree}} \quad (s3)$$

$$k_{sar} = \sqrt{\left(\frac{k_{rcon}}{k_{scon}}\right) \times \left(\frac{k_{\tau s}}{k_{\tau r}}\right) \times k_{\rho s}} \quad (s4)$$

where k_{lsmin} is the minimum observed leaf area to sapwood area ratio, k_{lsmax} is the maximum observed leaf area to sapwood area ratio, f_{Pgap} is the gap fraction calculated from the gap model, k_{rcon} is the hydraulic conductivity of roots, k_{scon} is the hydraulic conductivity of sapwood, $k_{\tau s}$ is the longevity of sapwood, and $k_{\tau r}$ is the root longevity.

Because of the different turnover rates in different biomass pools at each time step, the NPP allocation first ensures that the model adheres to the allometric relationships. The remaining NPP is then allocated for vegetation growth. To achieve the appropriate NPP allocation fraction for each biomass pool, we adjusted both the turnover rates and the allometric relationships.

Chave et al. (2010) collected leaf litterfall data from 81 sites across South America. After excluding data from short-statured, montane, and secondary tropical forests, we used the remaining 61 sites to calibrate the leaf turnover parameter in the model. Leaf turnover ($\Delta M_{c,l}$) is calculated at each time step (Δt) as a function of leaf age (Krinner et al., 2005):

$$\Delta M_{c,l} = M_{c,l} \times \min\left(0.99, f_{\tau l} \times \frac{\Delta t}{k_{\tau l}} \times \left(\frac{k_{la}}{k_{\tau l}}\right)^4\right) \quad (s5)$$

where k_{la} is the mean leaf age, $k_{\tau l}$ is the critical leaf age, and $f_{\tau l}$ is an empirical coefficient. After calibrating the model with the leaf litterfall data, the parameter $f_{\tau l}$ changed from 1 to 16. We also modified the relationship between leaf efficiency and leaf age following Chen et al. (2020).

We further adjusted the pipe model parameters to match the observed fractions of NPP allocation to leaves and wood from Yang et al. (2021). They developed a data assimilation model CAT (Carbon Assimilation in the Tropics) based on Bayesian formalism, which estimated NPP allocation fractions to leaves and wood, constrained by NPP, LAI, biomass, and SLA from both satellite and inventory data.

Initially, the modeled fraction of NPP allocated to leaves from the ORCHIDEE model

was 13.7% ± 0.3% (mean ± standard deviation), which was underestimated compared to observations (27.9% ± 3.1%, Fig. S6a). This underestimation is primarily due to the model's low estimation of leaf litterfall, with observed values of 3.0 ± 0.5 MgC/ha compared to 1.0 ± 0.2 MgC/ha in the ORCHIDEE model (Fig. S6b). After calibration, the modeled leaf litterfall increased to 3.1 ± 0.2 MgC/ha, aligning more closely with observations. Meanwhile, the modeled fraction of NPP allocated to leaves also increased to 29.2% ± 2.6%, close to the observation level. The modeled fraction of NPP allocated to wood remained consistent with observations, both before and after adjustment (Fig. S6c). All adjustments of parameters are summarized in Table S1.

Text S1.2 Wood density

In the ORCHIDEE model, wood density is a prescribed trait/parameter that influences both carbon allocation and tree diameter. A higher wood density leads to a lower value of the stem-to-leaf allocation factor f_{KF} (Eq. S3), which reduces leaf biomass and consequently lowers photosynthetic capacity. In addition, higher wood density results in smaller tree diameters and increased stem density (Eq. 2). Although empirical studies have shown that higher wood density is often associated with lower mortality rates (Esquivel-Muelbert et al., 2020), this relationship is not currently represented in the ORCHIDEE model.

Previously, the model applied a uniform wood density value for each PFT across all land areas. However, in the Amazon rainforest, wood density varies considerably, ranging from 0.4 gC/cm^3 to 0.8 gC/cm^3 (Mitchard et al., 2014). To account for this variation, we updated the model by incorporating a spatially explicit wood density map at a 1 km resolution, derived from four machine learning models, using the largest available wood density measurements (Yang et al., 2024).

Text S1.3 Hydraulic architecture and drought mortality

We merged ORCHIDEE-CAN-NHA r7236 into ORCHIDEE r8240. ORCHIDEE-CAN-NHA r7236 includes a plant hydraulic module that simulates leaf, stem, and root

water potential for each circumference class, and models tree mortality due to hydraulic failure by explicitly simulating the percentage loss of conductance (Yao et al., 2022). Although this drought-induced tree mortality differs from self-thinning mortality, during 2011-2020, it only impacted 25.2% of the grids in our analysis, leading to a 6.1% reduction in where it lowered the average biomass and a 10.1% reduction in mortality rates in these areas by 6.1% and 10.1%, respectively (Fig. S2). Overall, the AGB and biomass mortality rates are still predominantly controlled by α rather than drought-induced mortality during our study period.

Text S2: Active nitrogen content in the leaves

Given the limited observations available for accurately calibrating the nitrogen cycle in the Amazon rainforest, and the fact that tropical forests are generally not nitrogen-limited (Brookshire et al., 2012), we prescribed a leaf C/N ratio ($r_{c/n}$) of 25 (Sitch et al., 2003). We assumed that 10% of this nitrogen is allocated to structural tissues that do not contribute to V_{cmax}, and that the leaf nitrogen concentration profile within the canopy follows the distribution of light. The $M_{n,active}$ is calculated as:

$$M_{n,l}^{active} = M_{n,l} - M_{n,l}^{struc} = \frac{M_{c,l}}{r_{c/n}} - M_{c,l} \times 0.4\% \quad \text{(s6)}$$

where $M_{n,l}$ is the leaf nitrogen mass (gN m^{-2}), $M_{c,l}$ is the leaf carbon mass (gC m^{-2}), and $M_{n,l}^{struc}$ (gC m^{-2}) is the structural leaf nitrogen mass.

Text S3: Temporal variation and trend of AGB, GPP and biomass mortality rates

Our parameter optimization framework is not designed to capture interannual variation or long-term trends of GPP, AGB, or mortality. Here, we present the temporal dynamics of these variables for the period of 2001–2020 (Fig. S24). Currently, due to a lack of reliable observational data on the temporal variation or long-term trends of mortality and AGB, it's difficult to evaluate the model's performance on the temporal dynamics of mortality and AGB.

We compared the simulated GPP from the ORCHIDEE model with GPP from GOSIF

during this period. With spatially constant parameters and spatially varying parameters, the simulated multi-year regional mean GPP values from the ORCHIDEE model are 33.36±0.38 and 33.16±0.38 MgC ha^{-1} yr^{-1} (mean±standard deviation), respectively. The corresponding linear trends are 0.035 and 0.034 MgC ha^{-1} yr^{-2} ($p<0.05$), respectively (Fig. S24b). In comparison, the GOSIF-based multi-year regional mean GPP is 33.54±0.45 MgC ha^{-1} yr^{-1} with a trend of 0.049 MgC ha^{-1} yr^{-2} ($p<0.05$, Fig. S24b). The correlation coefficients between annual regional mean GPP from the GOSIF data and the ORCHIDEE model are 0.58 and 0.57 for spatially constant parameters and spatially varying parameters, respectively. These results suggest that the model can roughly capture the interannual variation and long-term trend of GPP from GOSIF, and our parameterization framework has only a minor influence on these temporal dynamics.

The linear trends of AGB from the ORCHIDEE model are also similar between the two configurations: 0.055 MgC ha^{-1} yr^{-1} ($p < 0.05$) for spatially constant parameters and 0.054 MgC ha^{-1} yr^{-1} ($p < 0.05$) for spatially varying parameters (Fig. S24a). The increasing trend in AGB is consistent with field observations, which indicate that intact Amazon forests continue to act as carbon sinks (Pan et al., 2024). No significant trend was found for biomass mortality rates over the same period ($p=0.65$ for simulations with spatially constant parameters and $p=0.67$ for simulations with spatially varying parameters; Fig. S24c), and there is no regional and long-term observational data of mortality for comparison.

Supplementary Figures

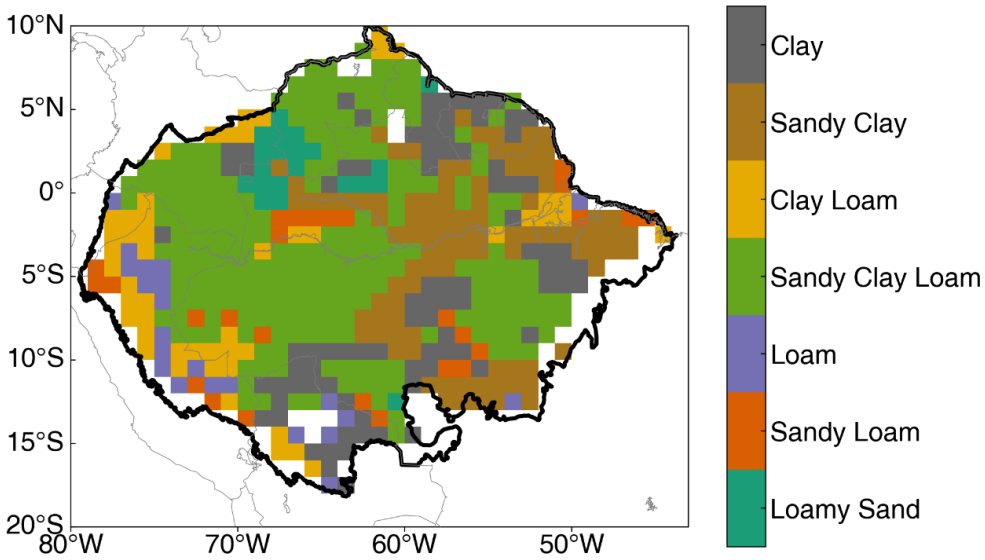

Figure S1. Soil texture map from Harmonized World Soils Database version 2.0 (HSWD2).

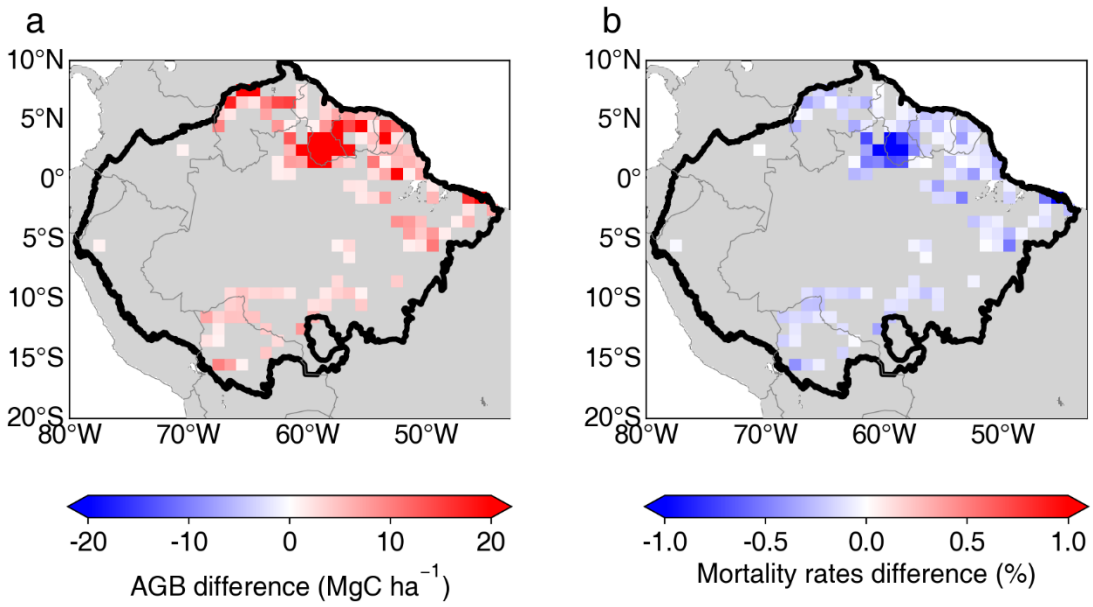

Figure S2. Spatial pattern of AGB (a) and biomass mortality rates (b) difference between simulations with and without drought mortality. 25.2% of grids are shown in the figure where the difference in AGB exceeds 1 MgC ha^{-1}.

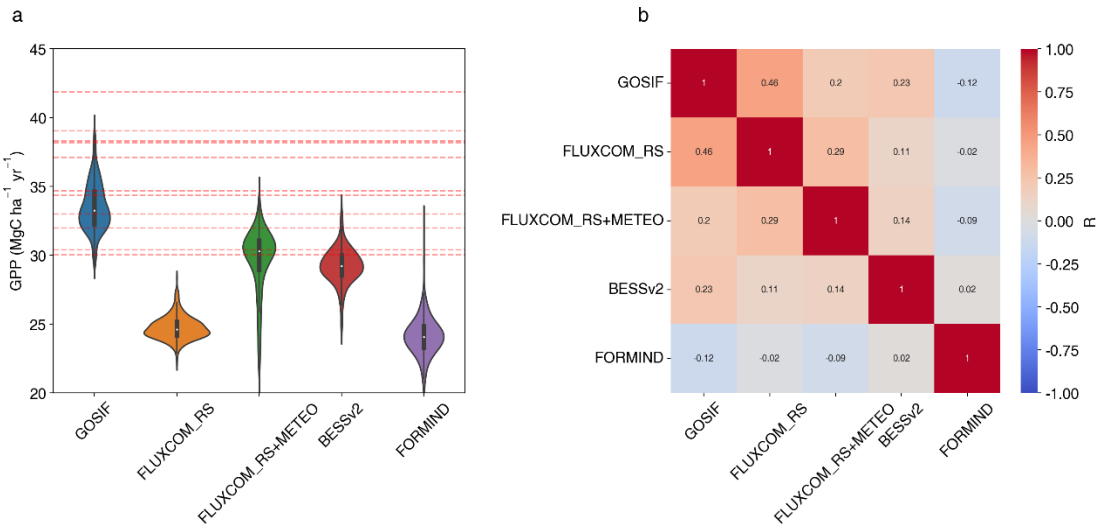

Figure S3. Five different GPP products in the Amazon basin (a) and their Pearson correlation coefficients (b). Red dashed lines represent GPP observations (Table S4) in the Amazon forest from Marthews et al. (2012) and Malhi et al. (2015). Sites with temperature lower than 18°C and annual mean precipitation below 1,500 mm were excluded from the GPP observations to be consistent with our study area.

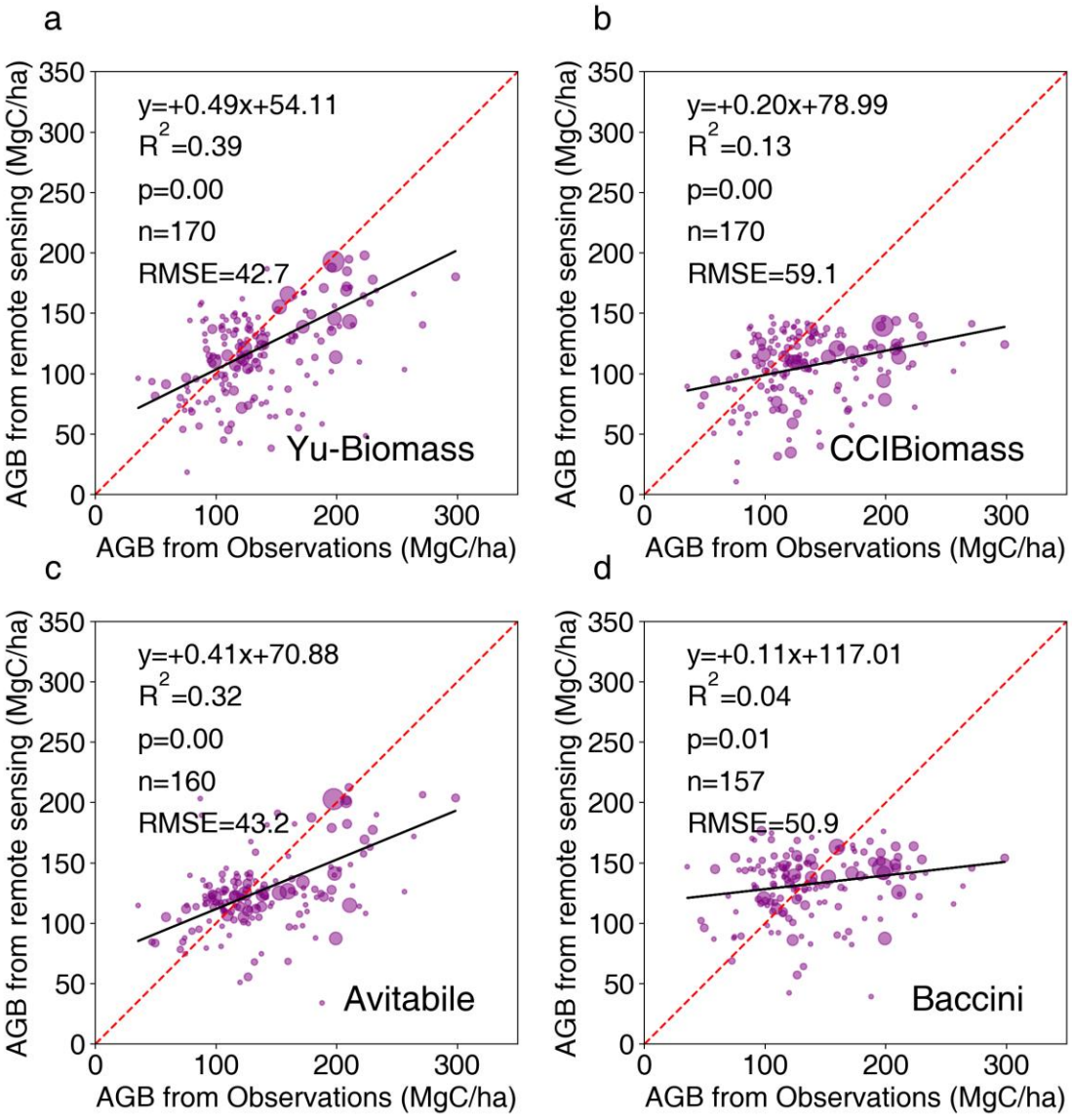

Figure S4. Relationship between above ground biomass (AGB) from field observations and AGB from remote sensing data at the resolution of 0.1° based on (a) Yu et al. (2023); (b) Santoro and Cartus (2024); (c) Avitabile et al. (2016); (d) Baccini et al. (2012). The size of the dots indicates the plot area. The dashed red line is the 1:1 line. The black solid line is the best fit between remote sensing data and observations weighted by plot area.

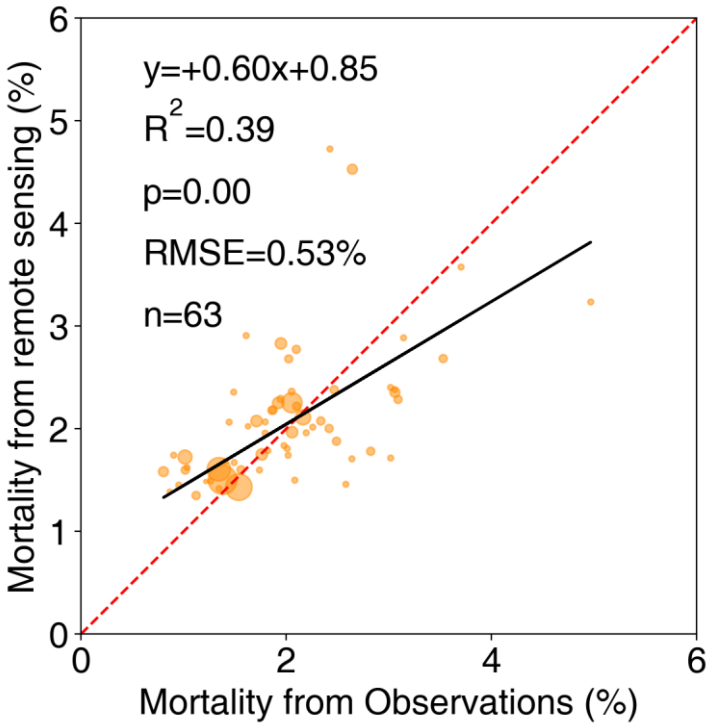

Figure S5. Relationship between mortality from field observations and mortality from remote sensing data at the resolution of 0.1°. The size of the dots indicates the plot area. The dashed red line is the 1:1 line. The black solid line is the best fit between remote sensing data and observations weighted by plot area.

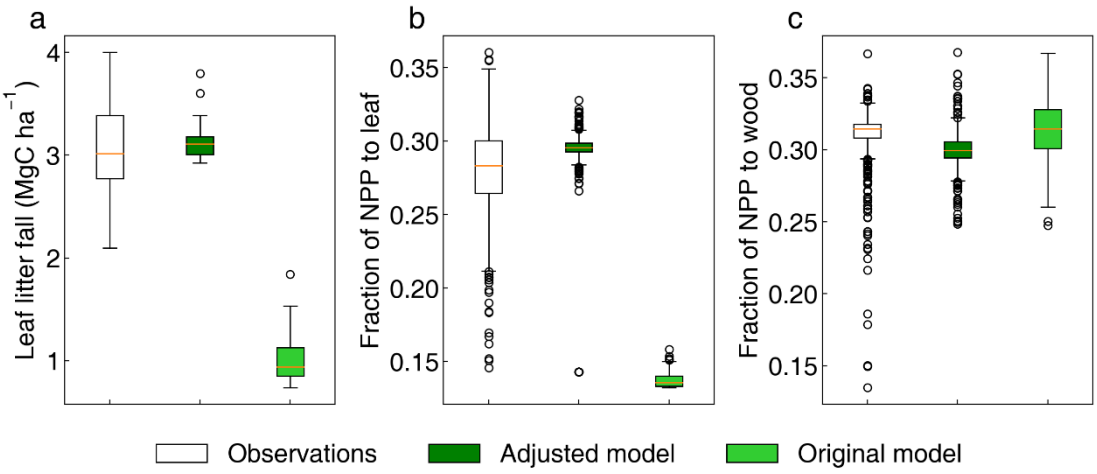

Figure S6. Calibration of carbon allocation. (a) Leaf litterfall; (b) Fraction of NPP allocated to leaf; (c) Fraction of NPP allocated to wood. Boxplots show the median, 25th, and 75th quantiles, with whiskers representing the maximum and minimum values excluding any outliers. Individual points are outliers.

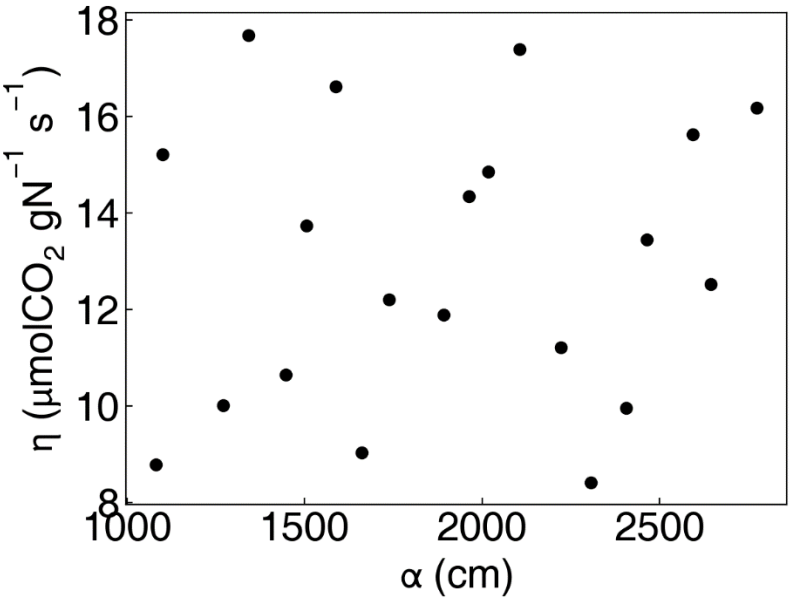

Figure S7. 20 sets of parameter values generated by Latin hypercube sampling.

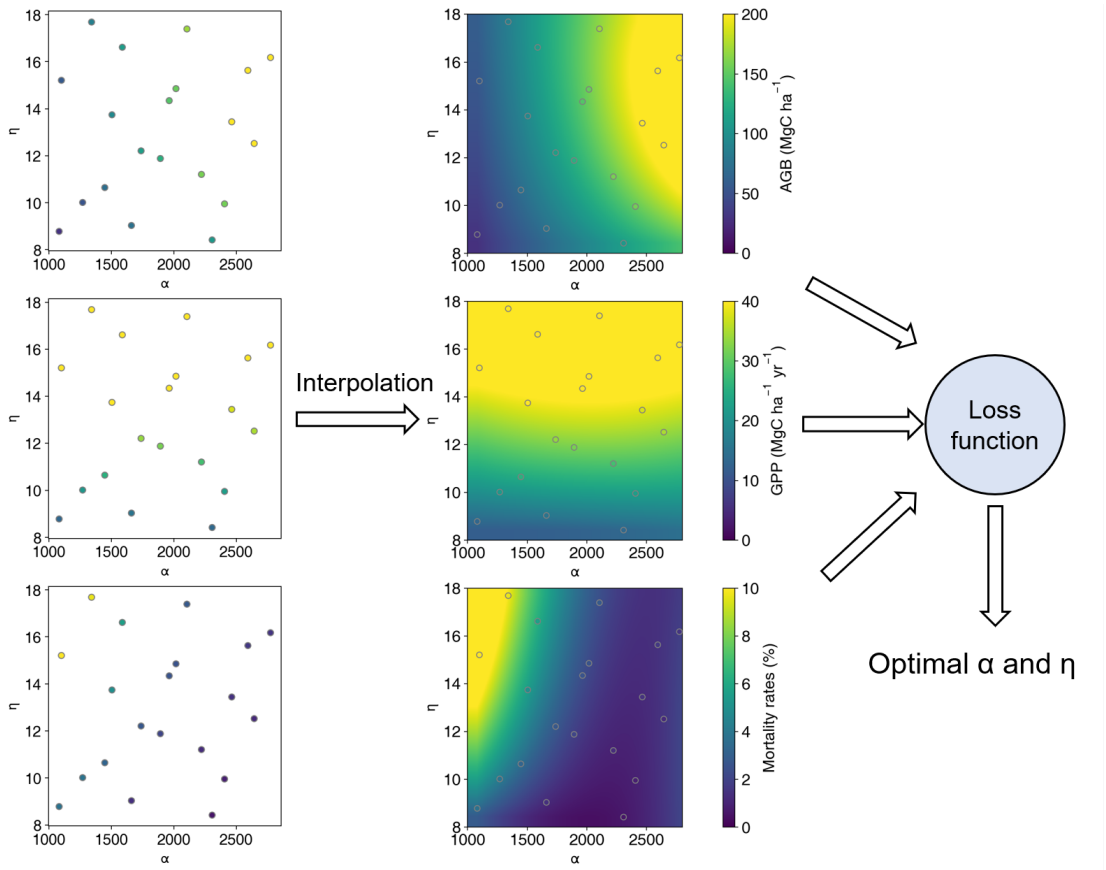

Figure S8. The schematic diagram for the interpolation method. We first collected the results of modeled AGB, GPP, and mortality rates based on the simulations from 20 sets of parameter values. Then we did the interpolation using quadratic splines over the whole parameter space. We finally found the optimal α and η based on the results from the interpolation and a loss function.

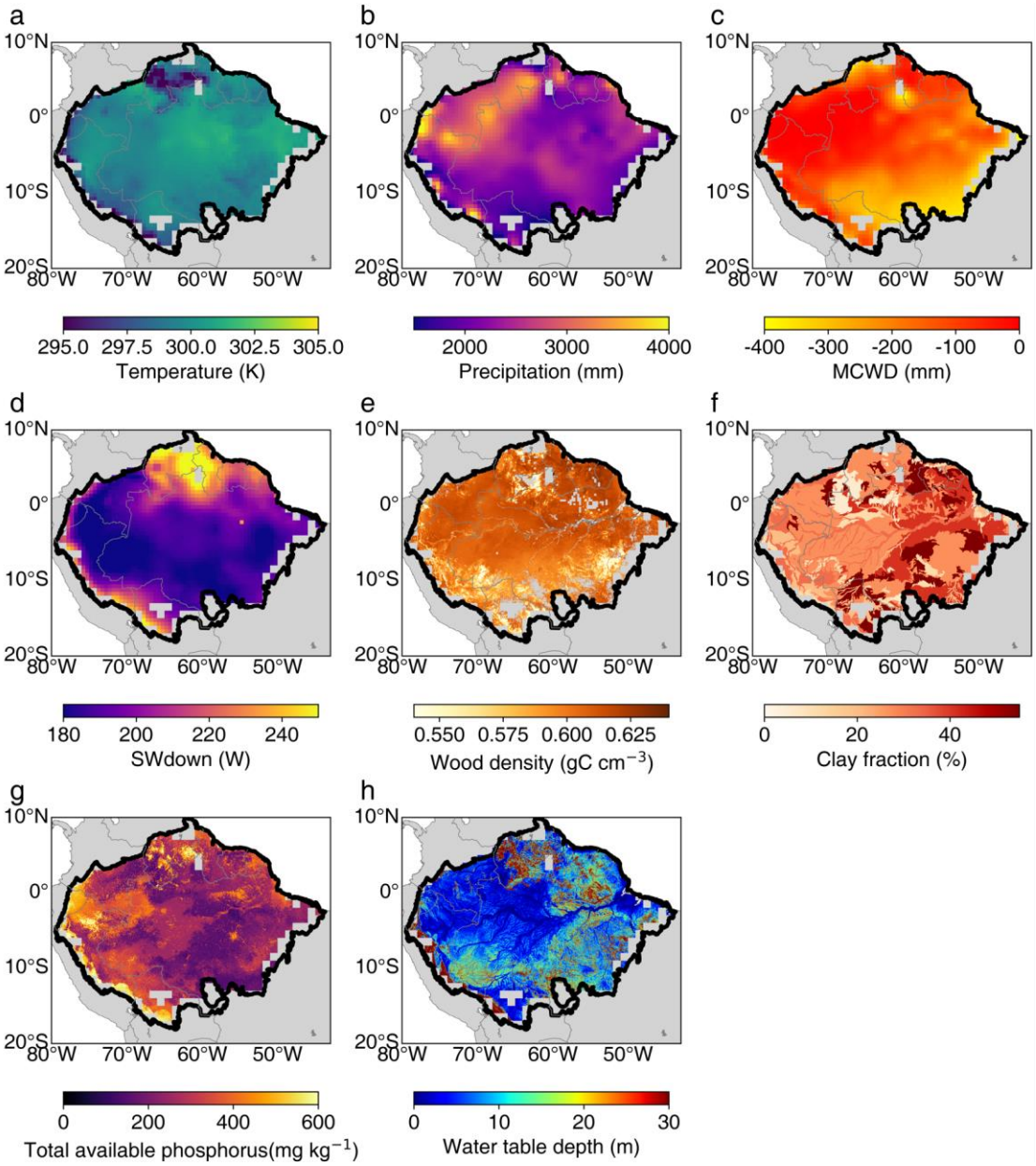

Figure S9. Maps of 8 explanatory variables at its original resolution. (a) Temperature; (b) precipitation; (c) maximum cumulative water deficit (MCWD); (d) downward shortwave radiation (SWdown); (e) wood density; (f) clay fraction; (g) total available phosphorous; (h) water table depth. The detailed information for each variable is listed in Table S3.

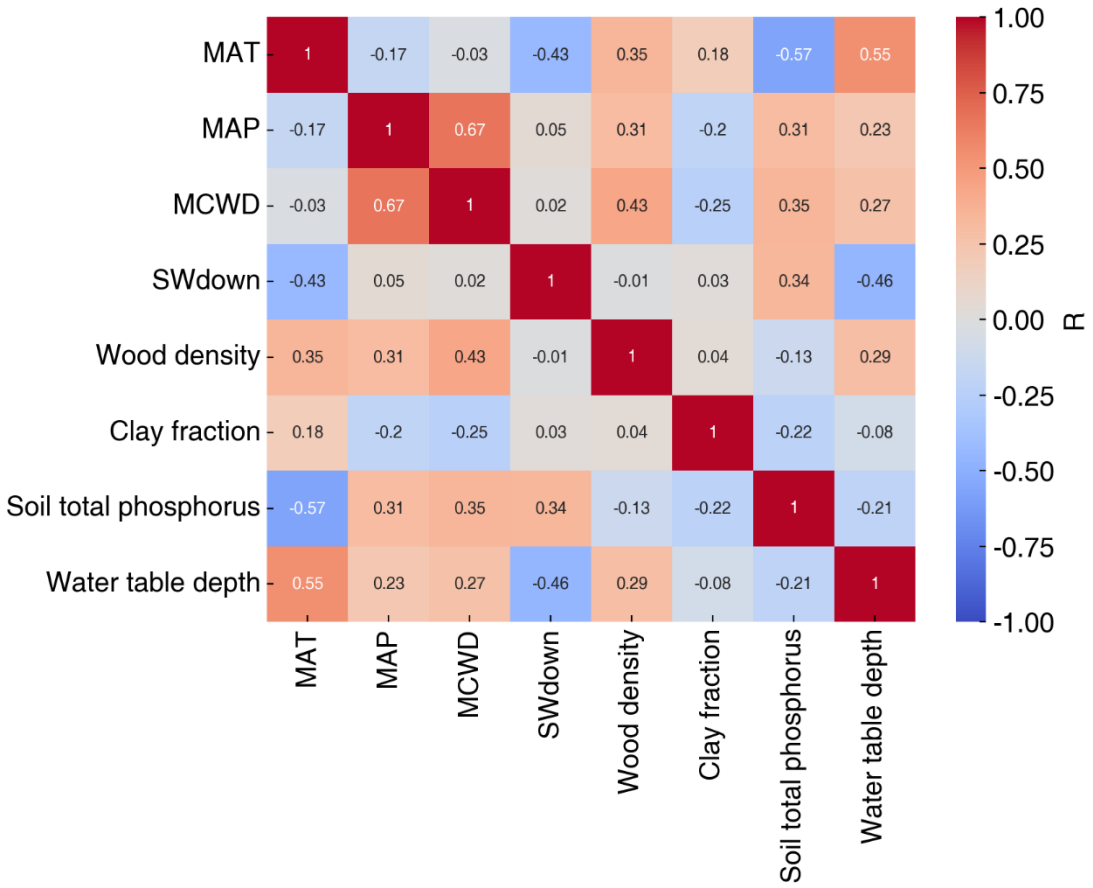

Figure S10. Correlation matrix for 8 explanatory variables.

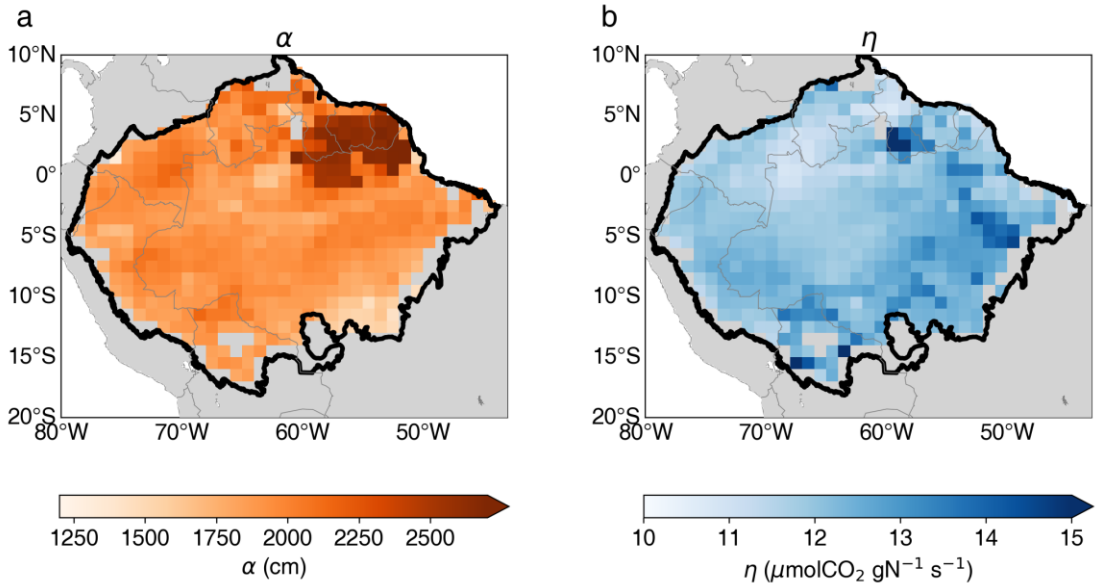

Figure S11. Spatial patterns of optimized spatially varying parameter maps of α (a) and η (b).

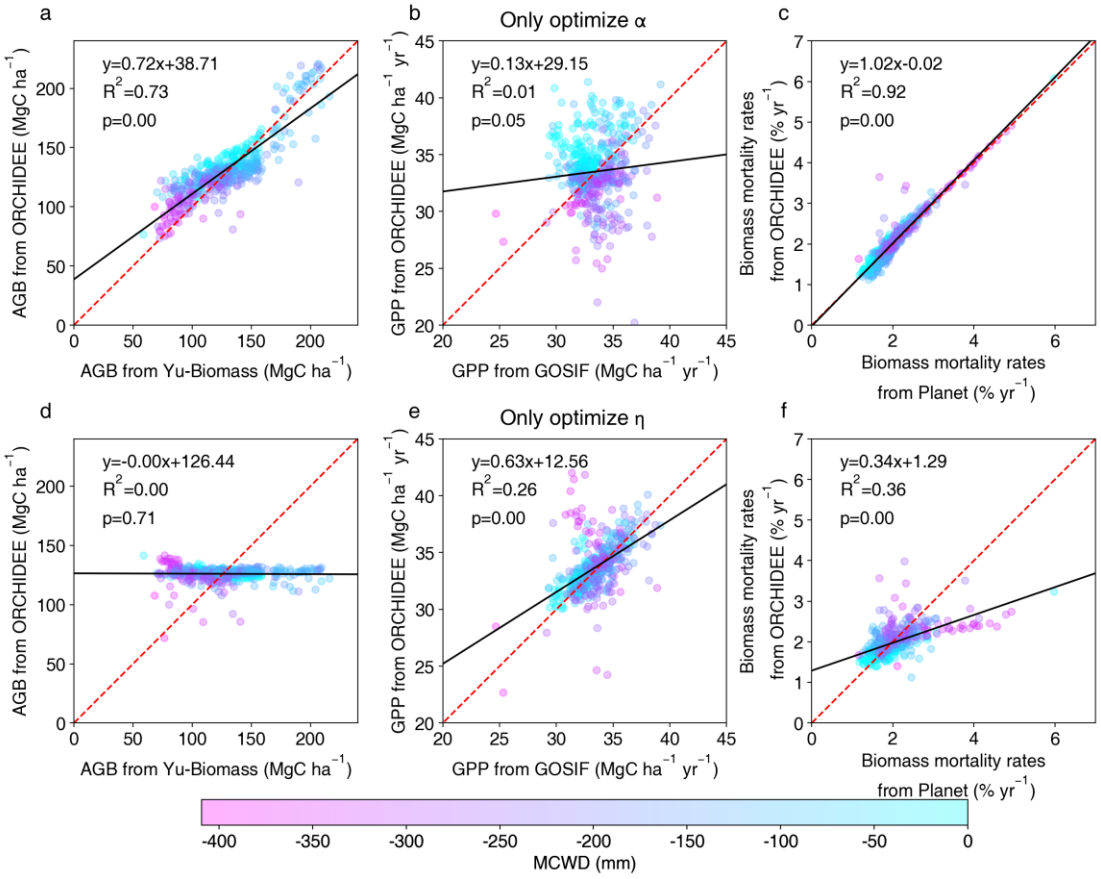

Figure S12. Comparison of model-simulated AGB, GPP, and biomass mortality rates with observations. Results from model simulation with spatially varying α and spatially constant η (a-c), and model with spatially varying η and spatially constant α (d-f). The dashed red line is the 1:1 line. The black solid line is the best fit between modeled results and observations. The color of the dots represents the value of MCWD to show its correlation with AGB, GPP, and biomass mortality rates.

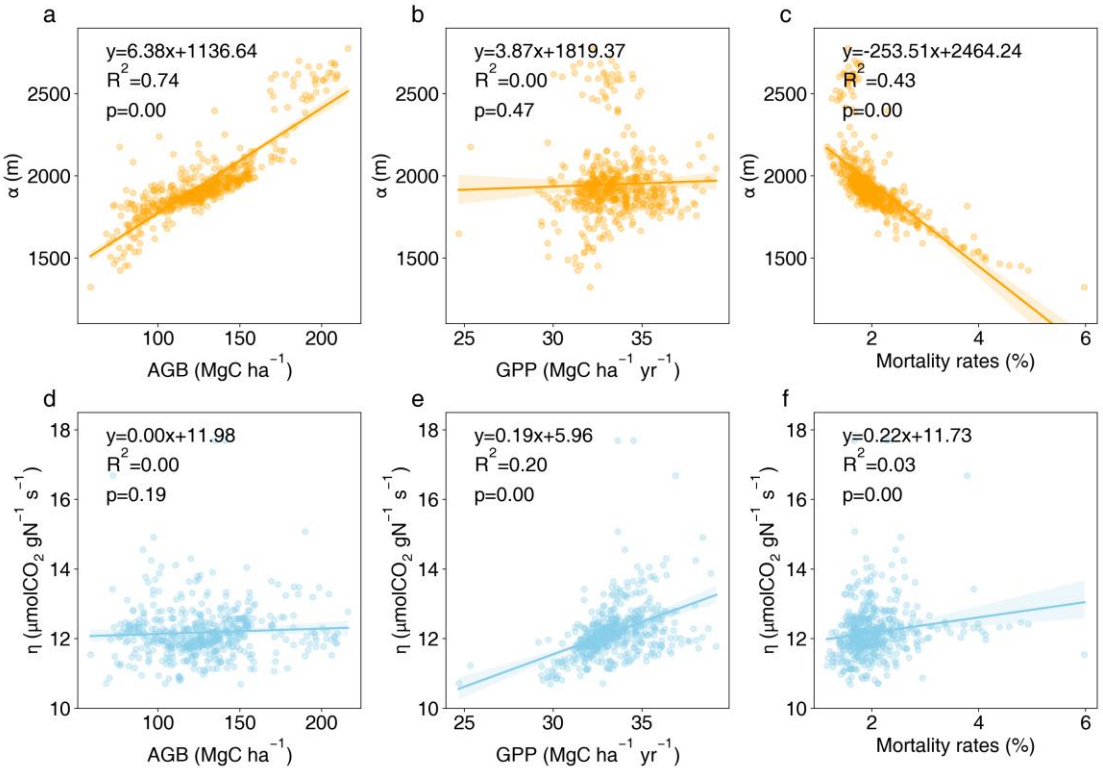

Figure S13. Relationship between spatially varying parameters and observations. (a-c) Spatially varying α versus AGB from Yu-Biomass (a), GOSIF GPP (b) mortality rates from Sassan (c). (d-f) Spatially varying η versus AGB from Yu-Biomass (d), GOSIF GPP (e) mortality rates from Sassan (f). The solid line is the best fit between observations and spatially varying parameters. The shaded area is the 95% confidence interval of the linear regression.

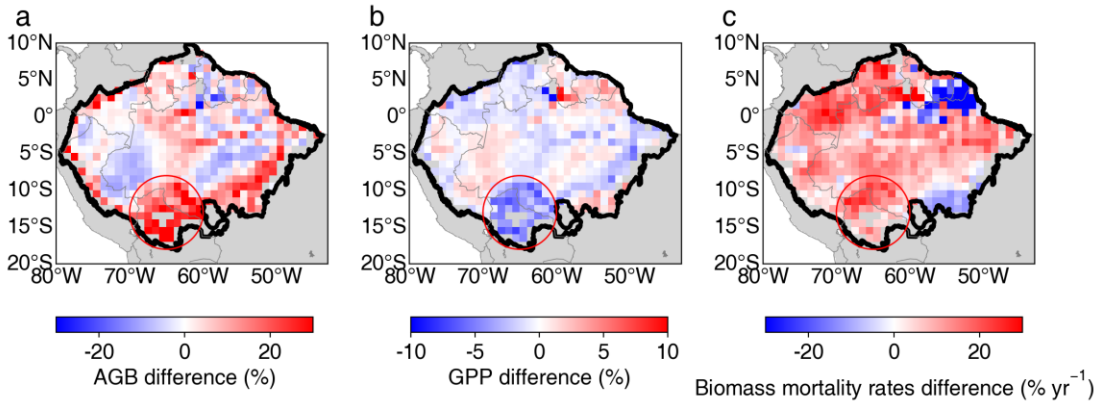

Figure S14. Spatial pattern of the differences between model-simulated results and observations. (a) Model-simulated AGB compared to AGB from Yu-Biomass, (b) Model-simulated GPP compared to GPP from GOSIF, and (c) Model-simulated biomass mortality rates compared to biomass mortality rates from Planet. The red circle highlights an example of grids where observational inconsistencies result in biases. In these grids, GPP is underestimated, while AGB and mortality rates are overestimated. If the model simulates higher GPP, the overestimation of mortality rates and AGB would increase further. These results reflect a trade-off during the optimization process.

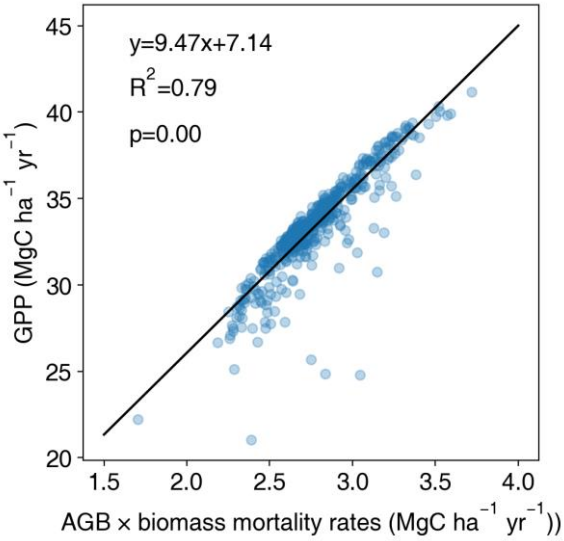

Figure S15. Relationship between model simulated GPP and AGB multiplied by biomass mortality rates.

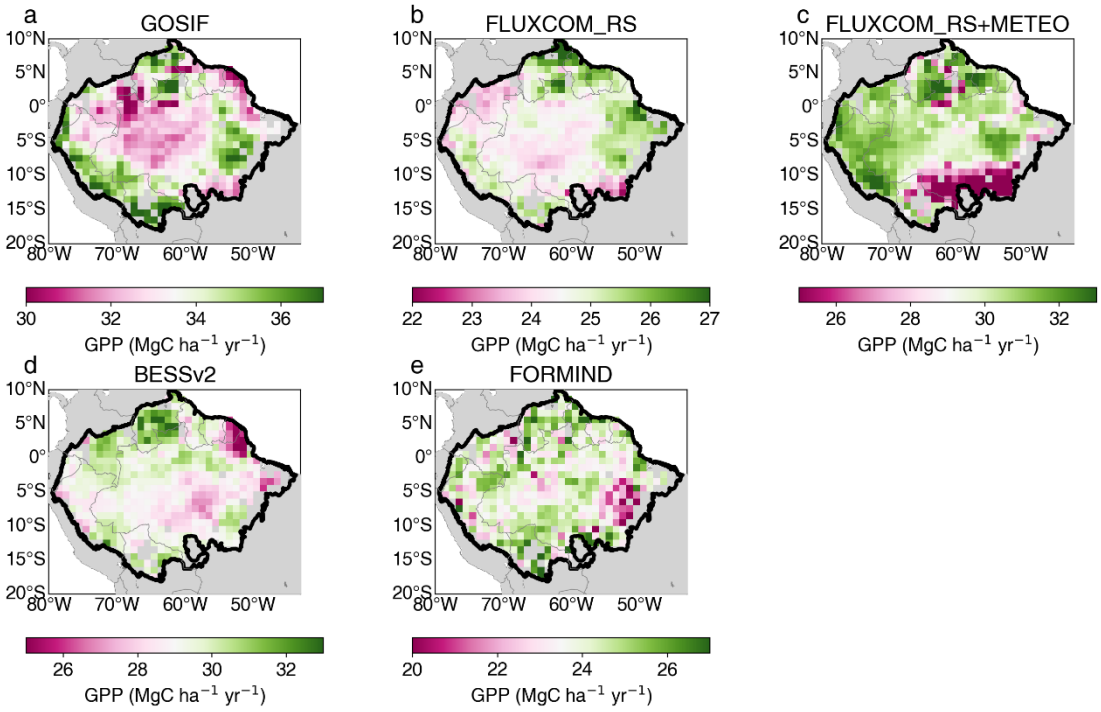

Figure S16. Spatial distributions of five GPP products used in this study: (a) GOSIF; (b) FLUXCOM_RS; (c) FLUXCOM_RS+METEO; (d) BESSv2; (e) FORMIND.

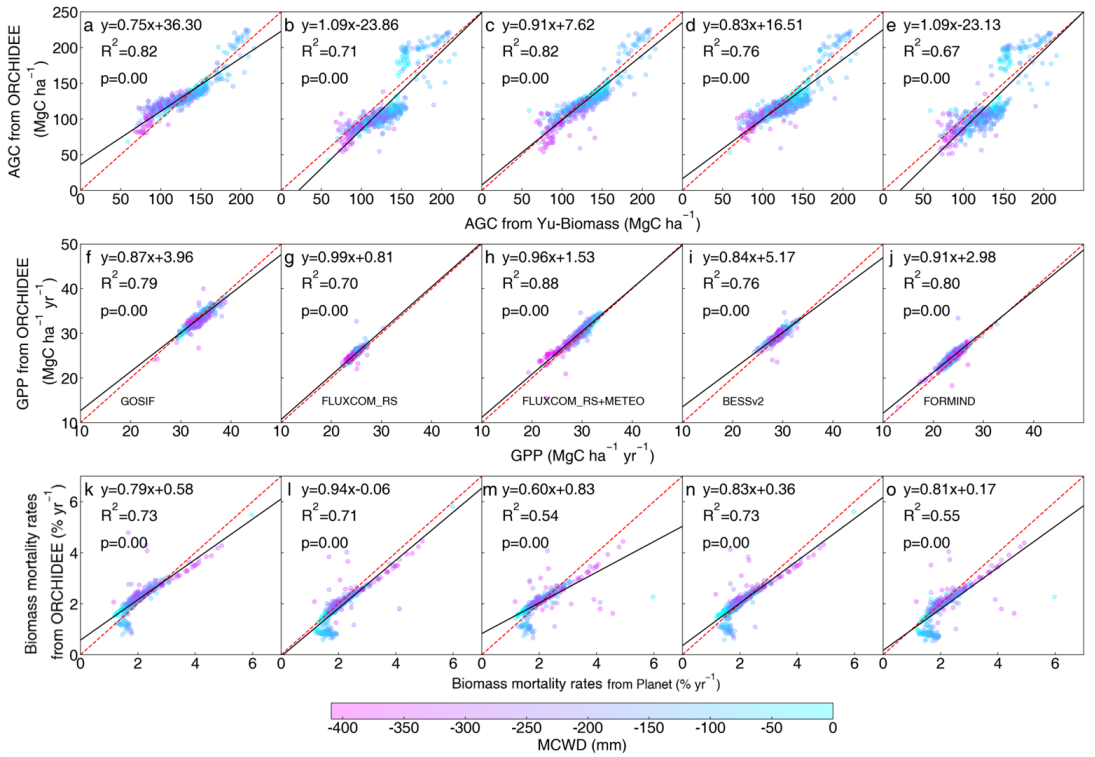

Figure S17. Same as Figure 3 but used different GPP observation datasets during the optimization. (a, f, k) Same as figure 2d-2f; (b, g, l) optimization results using FLUXCOM_RS GPP; (c, h, m) optimization results using FLUXCOM_RS+METEO GPP; (d, i, n) optimization results using BESSv2 GPP; (d, i, n) optimization results using FORMIND GPP. The dashed red line is the 1:1 line. The black solid line is the best fit between modeled results and observations.

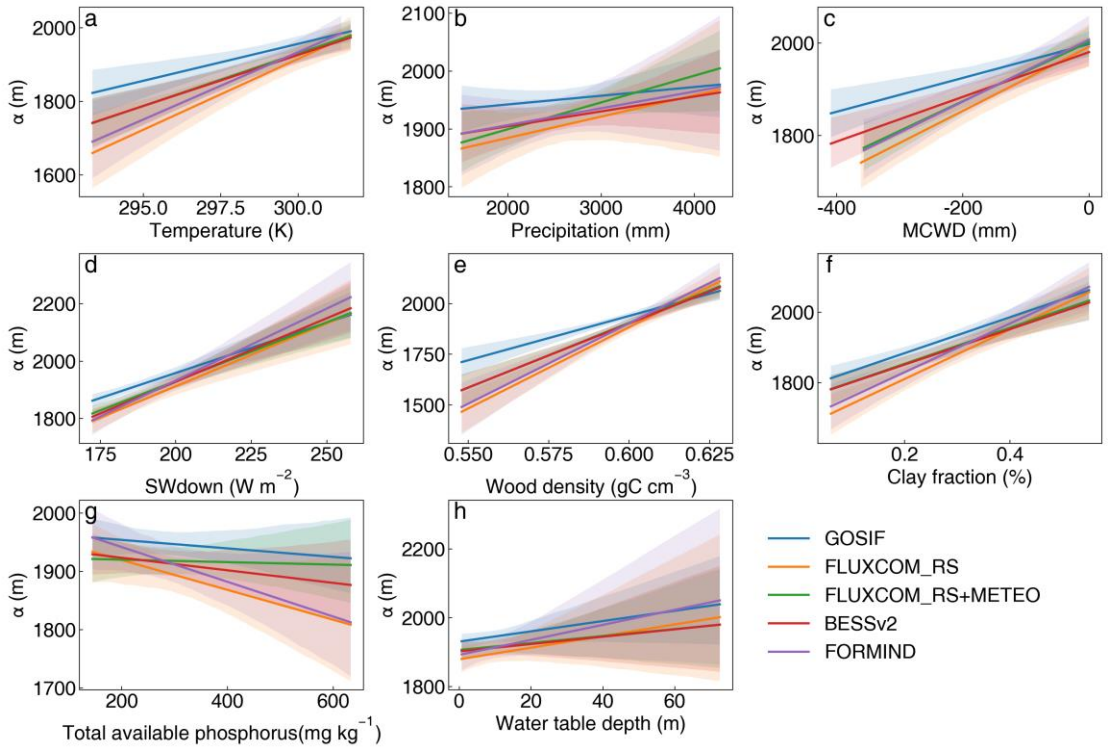

Figure S18 Impact of 8 explanatory variables on optimized parameters α using different GPP datasets: (a) temperature; (b) precipitation; (c) maximum cumulative water deficit (MCWD); (d) downward shortwave radiation (SWdown); (e) wood density; (f) clay fraction; (g) total available phosphorous; (h) water table depth. The solid line is the best fit between influencing factors and optimized parameters. The shaded area is the 95% confidence interval of the linear regression.

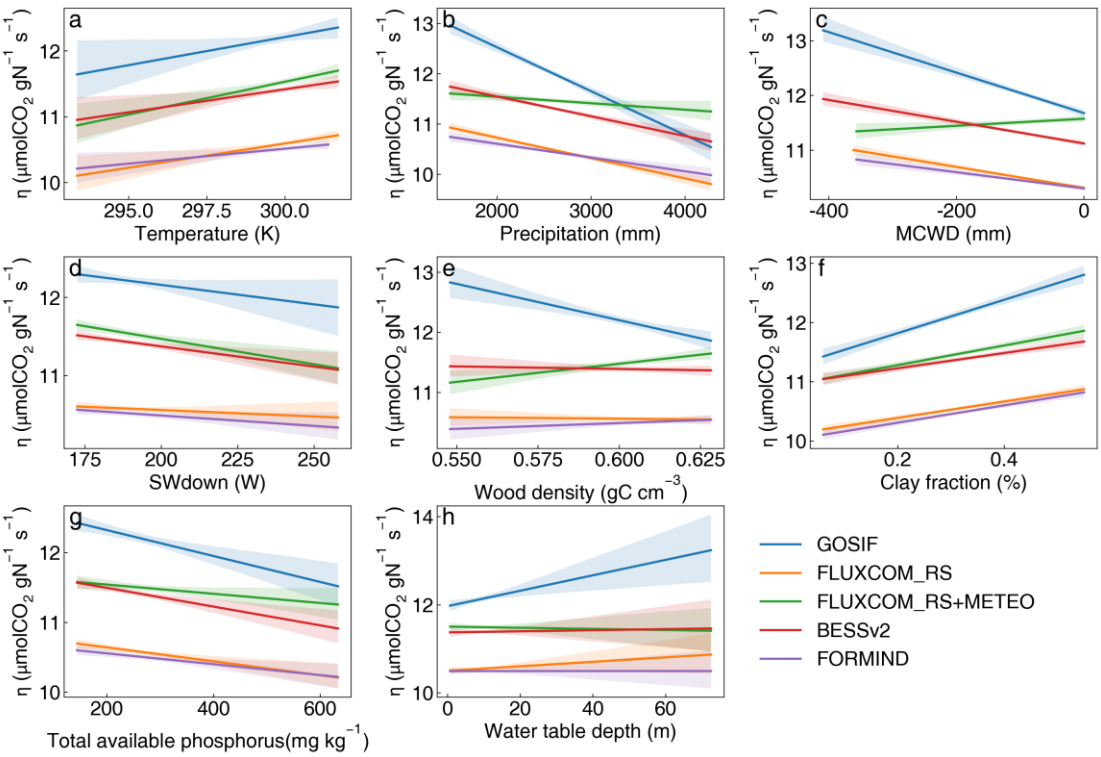

Figure S19. Same as Fig. S18 but for η.

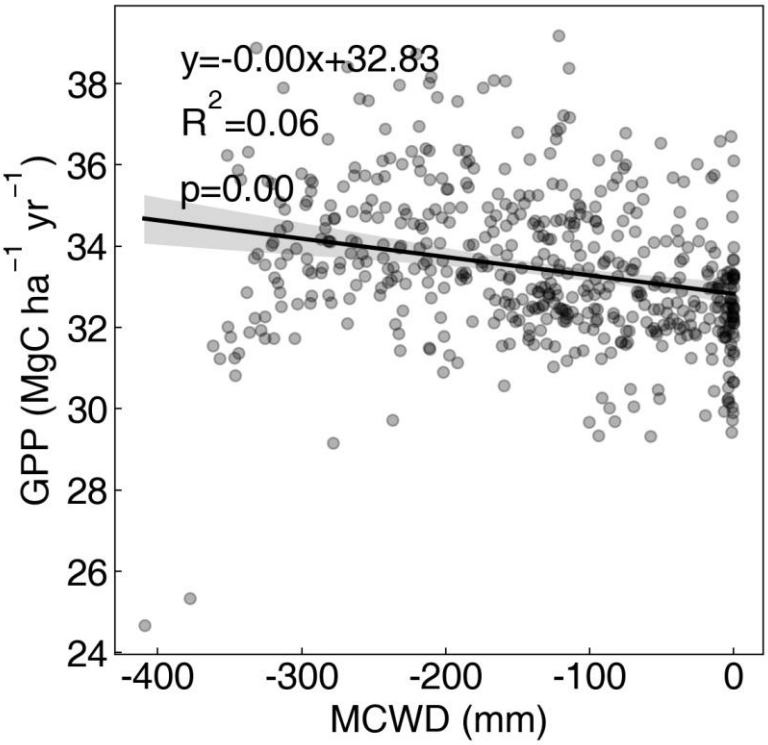

Figure S20. Relationship between MCWD from CRUJRA and GPP from GOSIF.

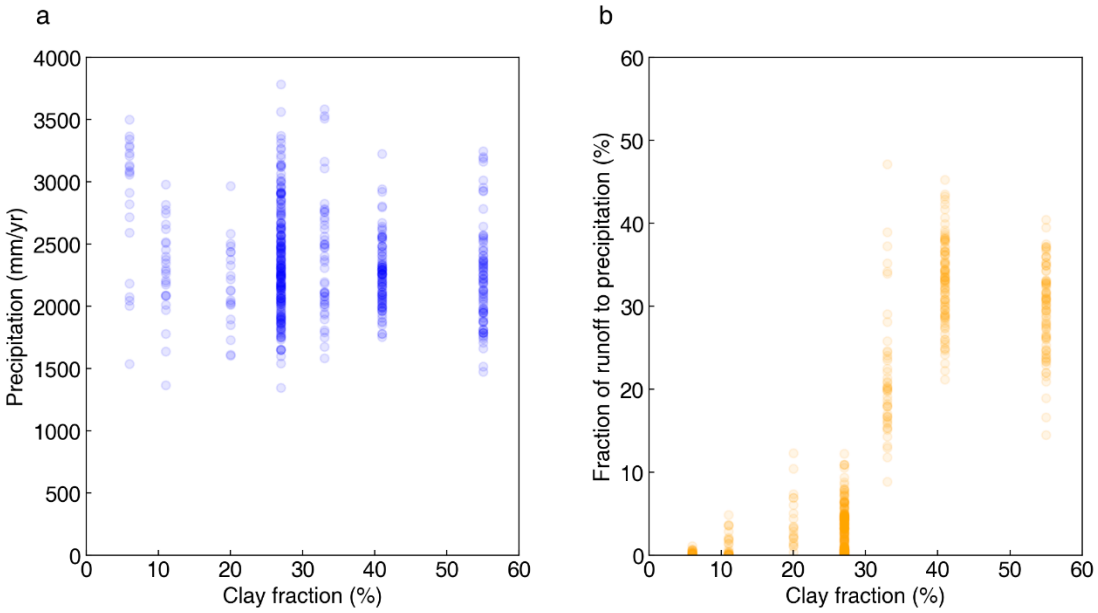

Figure S21. Impact of clay fraction on runoff. (a) Correlation between clay fraction and precipitation. (b) Correlation between clay fraction and the fraction of runoff relative to precipitation.

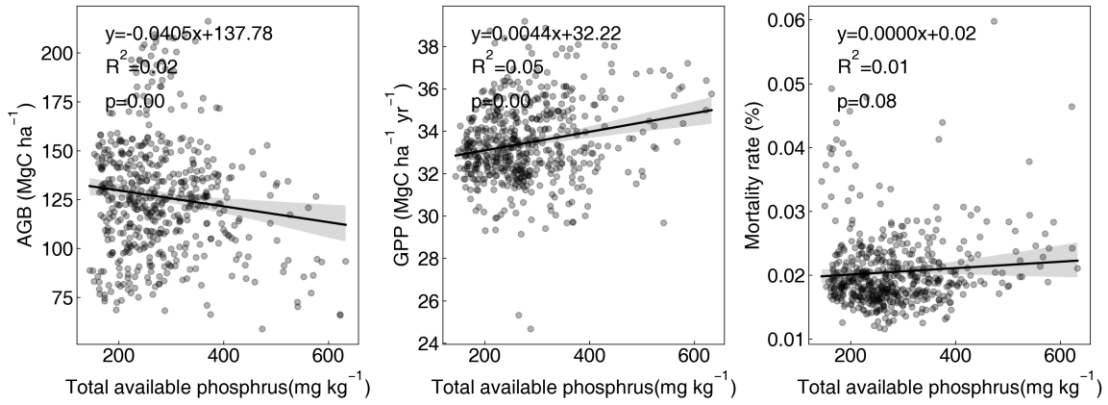

Figure S22. Relationship between total available phosphorus from CRUJRA and GPP from GOSIF.

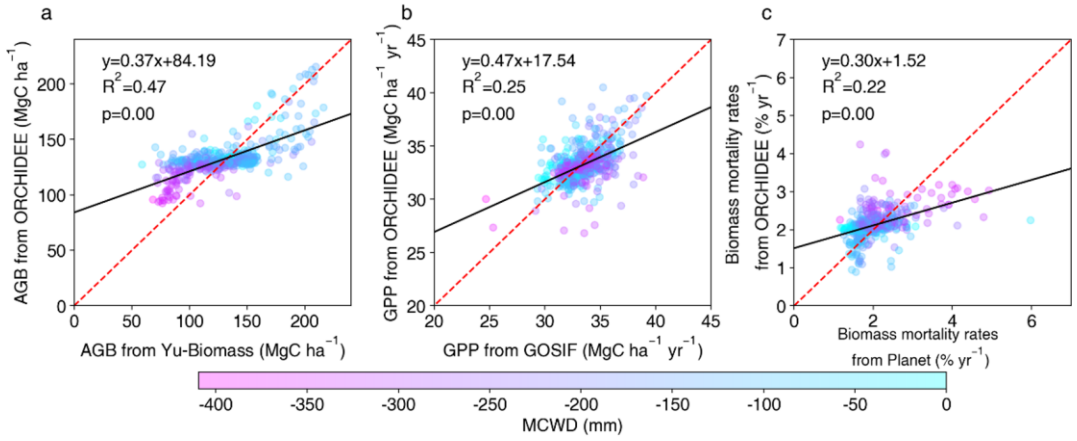

Figure S23. Same as Figure 3d-3f but using parameters α and η predicted by random forest regression to run the ORCHIDEE model.

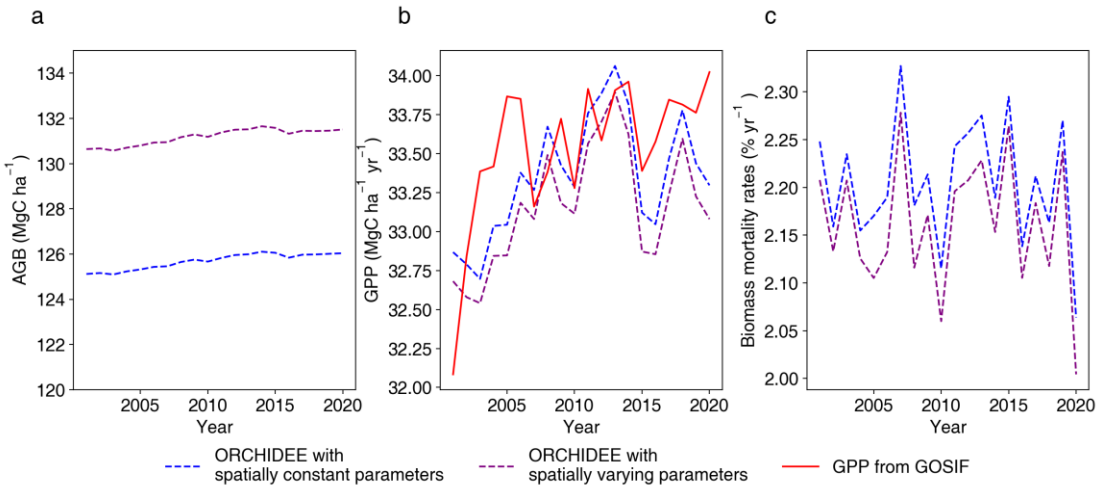

Figure S24. Temporal variation of regional mean AGB (a), GPP (b), and biomass mortality rates (c) from the ORCHIDEE model during 2001-2020. GPP from the GOSIF data is shown for comparison.

Supplementary Tables

Table S1 Modified parameters in the model

Symbol in the text (Symbol in ORCHIDEE model)	Unit	Default value	After modification	Description	Reference
k_{rcon} (k_belowgroud)	$m^3/kg/s/Mpa$	8.944E-08	4E-07	Belowground (roots + soil) specific conductivity	Yang et al., 2021
k_{lsmin} (k_latosa_min)	-	7500	10000	Minimum leaf-to-sapwood area ratio	Yang et al., 2021
$f_{\tau l}$ (turnover_C3)	-	1	16	Empirical coefficient for leaf turnover	Chave et al., 2010
α (alpha_self_thinning)	m	1941	spatially varying map	Coefficient of the self-thinning relationship	Santoro et al., 2023; Li et al., 2019; Yu et al., 2024
η (nue_opt)	$\mu molCO_2/gN/s$	14.08	spatially varying map	Nitrogen use efficiency of Vcmax	Santoro et al., 2023; Li et al., 2019; Yu et al., 2024
Wood density (pipe_density)	gC/m^3	287458	spatially varying map	Wood density	Yang et al., 2024
$r_{c/n}$ (cn_leaf)	gC/gN	16-45.5	25	CN ratio of leaves	Sitch et al., 2003

Table S2 Look-up table for 12 soil class properties defined by the United States Department of Agriculture (USDA). Ks: hydraulic conductivity at saturation; VG_n: Van Genuchten coefficients n; VG_a: Van Genuchten coefficients a; mcr: residual volumetric water content; mcs: saturated volumetric water content.

	Clay (%)	Silt (%)	Sand (%)	Ks (mm d^{-1})	VG_ n (-)	VG_a (mm^{-1})	mcr (m^3 m^{-3})	mcs (m^3 m^{-3})
Sand	3	4	93	7128.0	2.68	0.0145	0.045	0.43
Loamy Sand	6	13	81	3501.6	2.28	0.0124	0.057	0.41
Sandy Loam	11	26	63	1060.8	1.89	0.0075	0.065	0.41
Silt Loam	19	64	17	108.0	1.41	0.0020	0.067	0.45
Silt	10	84	6	60.0	1.37	0.0016	0.034	0.46
Loam	20	40	40	249.6	1.56	0.0036	0.078	0.43
Sandy Clay Loam	27	19	54	314.4	1.48	0.0059	0.1	0.39
Silty Clay Loam	33	59	8	16.8	1.23	0.0010	0.089	0.43
Clay Loam	33	37	30	62.4	1.31	0.0019	0.095	0.41
Sandy Clay	41	11	48	28.8	1.23	0.0027	0.1	0.38
Silty Clay	46	48	6	4.8	1.09	0.0005	0.07	0.36
Clay	55	30	15	48.0	1.09	0.0008	0.068	0.38

Table S3 List of the independent variables

Variable name	Unit	Original Resolution	Time	Data source
Mean annual temperature (MAT)	K	0.5°	2001-2020	CRUJRA2.4
Mean annual precipitation (MAP)	mm	0.5°	2001-2020	CRUJRA2.4
Maximum cumulative water deficit (MCWD)	mm	0.5°	2001-2020	CRUJRA2.4
Downward shortwave radiation (SWdown)	W/m^2	0.5°	2001-2020	CRUJRA2.4
Wood density	gC/cm^3	≈1 km	Historical	Yang et al., 2024
Clay fraction	%	≈1 km	Historical	HWSD2
Soil total phosphorus	mg/kg	≈10 km	Historical	Darela-Filho et al., 2024
Water table depth	m	≈1 km	Historical	Fan et al., 2013

Table S4 List of the GPP observation values used in Figure S3

Site name	GPP (MgC ha-1 yr-1)	Latitude	Longitude	Data source
San Pedro plot 1 (SPD-01)	30.03	13°2′ 56.89″ S	71°32′ 12.6″ W	Marthews et al., 2012
San Pedro plot 2 (SPD-02)	38.31	13°2′ 56.89″ S	71°32′ 12.6″ W	Marthews et al., 2012
Tambopata plot 3 (TAM-05)	37.11	12°50′18.59″ S	69°17′45.65″ W	Marthews et al., 2012
Tambopata plot 4 (TAM-06)	34.69	12°50′18.59″ S	69°17′45.65″ W	Marthews et al., 2012
Manaus, K34 Tower	30.4	2º35′21.08″ S	60º6′53.63″W	Marthews et al., 2012
Caxiuanã Tower plot (CAX-06)	38.2	1º43′11.26″ S	51º27′29.45 W	Marthews et al., 2012
Caxiuanã Tower plot (CAX-06)	33.0	1º43′11.26″ S	51º27′29.45 W	Marthews et al., 2012
Caxiuanã Tower plot (CAX-06)	32.0	1º43′11.26″ S	51º27′29.45 W	Marthews et al., 2012
Allpahuayo A (ALP11/ALP12)	39.05	3°57'0" S	73°26'0" W	Malhi et al., 2015
Allpahuayo C (ALP30)	41.88	3°57'15.48" S	73°25'36.12" W	Malhi et al., 2015
Caxiuanã Control plot (CAX-04)	34.37	1°42'57.60" S	51°27'25.20" W	Malhi et al., 2015

References

Avitabile, V., Herold, M., Heuvelink, G. B. M., Lewis, S. L., Phillips, O. L., Asner, G. P., Armston, J., Ashton, P. S., Banin, L. F., Bayol, N., Berry, N. J., Boeckx, P., de Jong, B. H. J., DeVries, B., Girardin, C. A. J., Kearsley, E., Lindsell, J. A., Lopez-Gonzalez, G., Lucas, R., Malhi, Y., Morel, A., Mitchard, E. T. A., Nagy, L., Qie, L., Quinones, M. J., Ryan, C. M., Ferry, S. J. W., Sunderland, T., Laurin, G. V., Gatti, R. C., Valentini, R., Verbeeck, H., Wijaya, A., Willcock, S., Asthon, P., Banin, L. F., Bayol, N., Berry, N. J., Boeckx, P., de Jong, B. H. J., DeVries, B., Girardin, C. A. J., Kearsley, E., Lindsell, J. A., Lopez-Gonzalez, G., Lucas, R., Malhi, Y., Morel, A., Mitchard, E. T. A., Nagy, L., Qie, L., Quinones, M. J., Ryan, C. M., Slik, F., Sunderland, T., Vaglio Laurin, G., Valentini, R., Verbeeck, H., Wijaya, A., and Willcock, S.: An integrated pan-tropical biomass map using multiple reference datasets, Global Change Biology, 22, 1406-1420, 10.1111/gcb.13139, 2016.

Baccini, A., Goetz, S. J., Walker, W. S., Laporte, N. T., Sun, M., Sulla-Menashe, D.,

Hackler, J., Beck, P. S. A., Dubayah, R., Friedl, M. A., Samanta, S., and Houghton, R. A.: Estimated carbon dioxide emissions from tropical deforestation improved by carbon-density maps, Nature Climate Change, 2, 182-185, 10.1038/nclimate1354, 2012.

Bastrikov, V., MacBean, N., Bacour, C., Santaren, D., Kuppel, S., and Peylin, P.: Land surface model parameter optimisation using in situ flux data: comparison of gradient-based versus random search algorithms (a case study using ORCHIDEE v1.9.5.2), Geosci. Model Dev., 11, 4739-4754, 10.5194/gmd-11-4739-2018, 2018.

Brookshire, E. N. J., Gerber, S., Menge, D. N. L., and Hedin, L. O.: Large losses of inorganic nitrogen from tropical rainforests suggest a lack of nitrogen limitation, Ecology Letters, 15, 9-16, https://doi.org/10.1111/j.1461-0248.2011.01701.x, 2012.

Chave, J., Navarrete, D., Almeida, S., Álvarez, E., Aragão, L. E. O. C., Bonal, D., Châtelet, P., Silva-Espejo, J. E., Goret, J. Y., von Hildebrand, P., Jiménez, E., Patiño, S., Peñuela, M. C., Phillips, O. L., Stevenson, P., and Malhi, Y.: Regional and seasonal patterns of litterfall in tropical South America, Biogeosciences, 7, 43-55, 10.5194/bg-7-43-2010, 2010.

Chen, X., Maignan, F., Viovy, N., Bastos, A., Goll, D., Wu, J., Liu, L., Yue, C., Peng, S., Yuan, W., da Conceição, A. C., O'Sullivan, M., and Ciais, P.: Novel Representation of Leaf Phenology Improves Simulation of Amazonian Evergreen Forest Photosynthesis in a Land Surface Model, Journal of Advances in Modeling Earth Systems, 12, e2018MS001565, https://doi.org/10.1029/2018MS001565, 2020.

Esquivel-Muelbert, A., Phillips, O. L., Brienen, R. J. W., Fauset, S., Sullivan, M. J. P., Baker, T. R., Chao, K.-J., Feldpausch, T. R., Gloor, E., Higuchi, N., Houwing-Duistermaat, J., Lloyd, J., Liu, H., Malhi, Y., Marimon, B., Marimon Junior, B. H., Monteagudo-Mendoza, A., Poorter, L., Silveira, M., Torre, E. V., Dávila, E. A., del Aguila Pasquel, J., Almeida, E., Loayza, P. A., Andrade, A., Aragão, L. E. O. C., Araujo-Murakami, A., Arets, E., Arroyo, L., Aymard C, G. A., Baisie, M., Baraloto, C., Camargo, P. B., Barroso, J., Blanc, L., Bonal, D., Bongers, F., Boot, R., Brown, F., Burban, B., Camargo, J. L., Castro, W., Moscoso, V. C., Chave, J., Comiskey, J., Valverde, F. C., da Costa, A. L., Cardozo, N. D., Di Fiore, A., Dourdain, A., Erwin, T., Llampazo, G. F., Vieira, I. C. G., Herrera, R., Honorio Coronado, E., Huamantupa-Chuquimaco, I., Jimenez-Rojas, E., Killeen, T., Laurance, S., Laurance, W., Levesley, A., Lewis, S. L., Ladvocat, K. L. L. M., Lopez-Gonzalez, G., Lovejoy, T., Meir, P., Mendoza, C., Morandi, P., Neill, D., Nogueira Lima, A. J., Vargas, P. N., de Oliveira, E. A., Camacho, N. P., Pardo, G., Peacock, J., Peña-Claros, M., Peñuela-Mora, M. C., Pickavance, G., Pipoly, J., Pitman, N., Prieto, A., Pugh, T. A. M., Quesada, C., Ramirez-Angulo, H., de Almeida Reis, S. M., Rejou-Machain, M., Correa, Z. R., Bayona, L. R., Rudas, A., Salomão, R., Serrano, J., Espejo, J. S., Silva, N., Singh, J., Stahl, C., Stropp, J., Swamy, V., Talbot, J., ter Steege, H., Terborgh, J., Thomas, R., Toledo, M., Torres-Lezama, A., Gamarra, L.

V., van der Heijden, G., van der Meer, P., van der Hout, P., Martinez, R. V., Vieira, S. A., Cayo, J. V., Vos, V., Zagt, R., Zuidema, P., and Galbraith, D.: Tree mode of death and mortality risk factors across Amazon forests, Nature Communications, 11, 5515, 10.1038/s41467-020-18996-3, 2020.

Krinner, G., Viovy, N., de Noblet-Ducoudré, N., Ogée, J., Polcher, J., Friedlingstein, P., Ciais, P., Sitch, S., and Prentice, I. C.: A dynamic global vegetation model for studies of the coupled atmosphere-biosphere system, Global Biogeochemical Cycles, 19, 10.1029/2003GB002199, 2005.

Malhi, Y., Doughty, C. E., Goldsmith, G. R., Metcalfe, D. B., Girardin, C. A. J., Marthews, T. R., del Aguila-Pasquel, J., Aragão, L. E. O. C., Araujo-Murakami, A., Brando, P., da Costa, A. C. L., Silva-Espejo, J. E., Farfán Amézquita, F., Galbraith, D. R., Quesada, C. A., Rocha, W., Salinas-Revilla, N., Silvério, D., Meir, P., and Phillips, O. L.: The linkages between photosynthesis, productivity, growth and biomass in lowland Amazonian forests, Global Change Biology, 21, 2283-2295, https://doi.org/10.1111/gcb.12859, 2015.

Marthews, T. R., Malhi, Y., Girardin, C. A. J., Silva Espejo, J. E., Aragão, L. E. O. C., Metcalfe, D. B., Rapp, J. M., Mercado, L. M., Fisher, R. A., Galbraith, D. R., Fisher, J. B., Salinas-Revilla, N., Friend, A. D., Restrepo-Coupe, N., and Williams, R. J.: Simulating forest productivity along a neotropical elevational transect: temperature variation and carbon use efficiency, Global Change Biology, 18, 2882-2898, https://doi.org/10.1111/j.1365-2486.2012.02728.x, 2012.

Mitchard, E. T. A., Feldpausch, T. R., Brienen, R. J. W., Lopez-Gonzalez, G., Monteagudo, A., Baker, T. R., Lewis, S. L., Lloyd, J., Quesada, C. A., Gloor, M., Ter Steege, H., Meir, P., Alvarez, E., Araujo-Murakami, A., Aragão, L. E. O. C., Arroyo, L., Aymard, G., Banki, O., Bonal, D., Brown, S., Brown, F. I., Cerón, C. E., Chama Moscoso, V., Chave, J., Comiskey, J. A., Cornejo, F., Corrales Medina, M., Da Costa, L., Costa, F. R. C., Di Fiore, A., Domingues, T. F., Erwin, T. L., Frederickson, T., Higuchi, N., Honorio Coronado, E. N., Killeen, T. J., Laurance, W. F., Levis, C., Magnusson, W. E., Marimon, B. S., Marimon Junior, B. H., Mendoza Polo, I., Mishra, P., Nascimento, M. T., Neill, D., Núñez Vargas, M. P., Palacios, W. A., Parada, A., Pardo Molina, G., Peña-Claros, M., Pitman, N., Peres, C. A., Poorter, L., Prieto, A., Ramirez-Angulo, H., Restrepo Correa, Z., Roopsind, A., Roucoux, K. H., Rudas, A., Salomão, R. P., Schietti, J., Silveira, M., de Souza, P. F., Steininger, M. K., Stropp, J., Terborgh, J., Thomas, R., Toledo, M., Torres-Lezama, A., van Andel, T. R., van der Heijden, G. M. F., Vieira, I. C. G., Vieira, S., Vilanova-Torre, E., Vos, V. A., Wang, O., Zartman, C. E., Malhi, Y., and Phillips, O. L.: Markedly divergent estimates of Amazon forest carbon density from ground plots and satellites, Global ecology and biogeography : a journal of macroecology, 23, 935-946, 10.1111/geb.12168, 2014.

Naudts, K., Ryder, J., McGrath, M. J., Otto, J., Chen, Y., Valade, A., Bellasen, V., Berhongaray, G., Bönisch, G., Campioli, M., Ghattas, J., De Groote, T., Haverd, V., Kattge, J., MacBean, N., Maignan, F., Merilä, P., Penuelas, J., Peylin, P., Pinty,

B., Pretzsch, H., Schulze, E. D., Solyga, D., Vuichard, N., Yan, Y., and Luyssaert, S.: A vertically discretised canopy description for ORCHIDEE (SVN r2290) and the modifications to the energy, water and carbon fluxes, Geoscientific Model Development, 8, 2035-2065, 10.5194/gmd-8-2035-2015, 2015.

Pan, Y., Birdsey, R. A., Phillips, O. L., Houghton, R. A., Fang, J., Kauppi, P. E., Keith, H., Kurz, W. A., Ito, A., Lewis, S. L., Nabuurs, G.-J., Shvidenko, A., Hashimoto, S., Lerink, B., Schepaschenko, D., Castanho, A., and Murdiyarso, D.: The enduring world forest carbon sink, Nature, 631, 563-569, 10.1038/s41586-024-07602-x, 2024.

Raoult, N., Beylat, S., Salter, J. M., Hourdin, F., Bastrikov, V., Ottlé, C., and Peylin, P.: Exploring the potential of history matching for land surface model calibration, Geosci. Model Dev., 17, 5779-5801, 10.5194/gmd-17-5779-2024, 2024.

Santoro, M. and Cartus, O.: ESA Biomass Climate Change Initiative (Biomass_cci): Global datasets of forest above-ground biomass for the years 2010, 2015, 2016, 2017, 2018, 2019, 2020 and 2021, v5. NERC EDS Centre for Environmental Data Analysis [dataset], 10.5285/5f331c418e9f4935b8eb1b836f8a91b8, 2024.

Shinozaki, K. K. Y., Hozumi, K., and Kira, T.: A quantitative analysis of plant form—the pipe model theory. I. Basic analysis, Jpn.j.ecol, 1964.

Sitch, S., Smith, B., Prentice, I. C., Arneth, A., Bondeau, A., Cramer, W., Kaplan, J. O., Levis, S., Lucht, W., Sykes, M. T., Thonicke, K., and Venevsky, S.: Evaluation of ecosystem dynamics, plant geography and terrestrial carbon cycling in the LPJ dynamic global vegetation model, Global Change Biology, 9, 161-185, 10.1046/j.1365-2486.2003.00569.x, 2003.

Yang, H., Ciais, P., Wang, Y., Huang, Y., Wigneron, J.-P., Bastos, A., Chave, J., Chang, J., E. Doughty, C., Fan, L., Goll, D., Joetzjer, E., Li, W., Lucas, R., Quegan, S., Le Toan, T., and Yu, K.: Variations of carbon allocation and turnover time across tropical forests, Global Ecology and Biogeography, 30, 1271-1285, https://doi.org/10.1111/geb.13302, 2021.

Yang, H., Wang, S., Son, R., Lee, H., Benson, V., Zhang, W., Zhang, Y., Zhang, Y., Kattge, J., Boenisch, G., Schepaschenko, D., Karaszewski, Z., Stereńczak, K., Moreno-Martínez, Á., Nabais, C., Birnbaum, P., Vieilledent, G., Weber, U., and Carvalhais, N.: Global patterns of tree wood density, Global Change Biology, 30, e17224, https://doi.org/10.1111/gcb.17224, 2024.

Yao, Y., Joetzjer, E., Ciais, P., Viovy, N., Cresto Aleina, F., Chave, J., Sack, L., Bartlett, M., Meir, P., Fisher, R., and Luyssaert, S.: Forest fluxes and mortality response to drought: model description (ORCHIDEE-CAN-NHA r7236) and evaluation at the Caxiuanã drought experiment, Geoscientific Model Development, 15, 7809-7833, 10.5194/gmd-15-7809-2022, 2022.

Yu, Y., Saatchi, S., Yang, Y., Xu, L., and Meyer, V.: Mapping Global Live Woody Vegetation Biomass at Optimum Spatial Resolutions [dataset], https://doi.org/10.5281/zenodo.7583611, 2023.